


RESEARCH ARTICLE

Integrated DNA methylation analysis reveals a potential role for PTPRN2 in Marfan syndrome scoliosis

Zhen-zhong Zheng^{1,2} | Jing-hong Xu^{1,2} | Jia-lin Chen^{1,2} | Bin Jiang^{1,2} |
Hong Ma^{1,2} | Lei Li^{1,2} | Ya-wei Li^{1,2} | Yu-liang Dai^{1,2} | Bing Wang^{1,2} 

¹Department of Spine Surgery, The Second Xiangya Hospital, Central South University, Changsha, China

²Hunan Digital Spine Research Institute, Central South University, Changsha, China

Correspondence

Bing Wang and Yu-liang Dai, Department of Spine Surgery, The Second Xiangya Hospital of Central South University, 139 Ren Min Zhong Road, Changsha, Hunan 410011, China.

Email: wbyeyy@csu.edu.cn;
squaer_d@hotmail.com

Funding information

Hunan Province Science Foundation of China, Grant/Award Number: 2021JJ30938; Hunan Provincial Key Research and Development Program, Grant/Award Number: 2021SK2002

Abstract

Background: Marfan syndrome (MFS) is a rare genetic disorder caused by mutations in the Fibrillin-1 gene (FBN1) with significant clinical features in the skeletal, cardio-pulmonary, and ocular systems. To gain deeper insights into the contribution of epigenetics in the variability of phenotypes observed in MFS, we undertook the first analysis of integrating DNA methylation and gene expression profiles in whole blood from MFS and healthy controls (HCs).

Methods: The Illumina 850K (EPIC) DNA methylation array was used to detect DNA methylation changes on peripheral blood samples of seven patients with MFS and five HCs. Associations between methylation levels and clinical features of MFS were analyzed. Subsequently, we conducted an integrated analysis of the outcomes of the transcriptome data to analyze the correlation between differentially methylated positions (DMPs) and differentially expressed genes (DEGs) and explore the potential role of methylation-regulated DEGs (MeDEGs) in MFS scoliosis. The weighted gene co-expression network analysis was used to find gene modules with the highest correlation coefficient with target MeDEGs to annotate their functions in MFS.

Results: Our study identified 1253 DMPs annotated to 236 genes that were primarily associated with scoliosis, cardiomyopathy, and vital capacity. These conditions are typically associated with reduced lifespan in untreated MFS. We calculated correlations between DMPs and clinical features, such as Cobb angle to evaluate scoliosis and FEV1% to assess pulmonary function. Notably, cg20223687 (PTPRN2) exhibited a positive correlation with Cobb angle of scoliosis, potentially playing a role in ERKs inactivation.

Conclusions: Taken together, our systems-level approach sheds light on the contribution of epigenetics to MFS and offers a plausible explanation for the complex phenotypes that are linked to reduced lifespan in untreated MFS patients.

KEYWORDS

DNA methylation, gene expression profiles, Marfan syndrome, scoliosis, translational research

Bing Wang and Yu-liang Dai jointly supervised this work and contributed equally.

This is an open access article under the terms of the [Creative Commons Attribution-NonCommercial-NoDerivs](https://creativecommons.org/licenses/by-nc-nd/4.0/) License, which permits use and distribution in any medium, provided the original work is properly cited, the use is non-commercial and no modifications or adaptations are made.

© 2024 The Authors. *JOR Spine* published by Wiley Periodicals LLC on behalf of Orthopaedic Research Society.

1 | INTRODUCTION

Marfan syndrome (MFS) is a connective tissue disease that affects an estimated 1 in 5000 individuals and is inherited in an autosomal dominant pattern.¹ Mutations in the *FBN1* gene, responsible for encoding the extracellular matrix constituent fibrillin-1, have been identified as the cause of this condition. This protein is responsible for forming microfibrils, complex structures that provide tissues with both elasticity and structural support.²

The clinical presentation of MFS is distinguished by an extensive spectrum of phenotypic manifestations, encompassing features like bone abnormalities, skin anomalies, respiratory complications, ocular impairments, joint laxity, spinal cord defects, and cardiovascular system dysfunctions.³ Previous studies were mainly focused on the cardiovascular system, which causes death in MFS patients throughout their lives.³ However, untreated scoliosis also impairs cardiorespiratory functions and has a prominent effect on lifespan reduction.⁴ Scoliosis can decrease chest wall compliance and indirectly reduce lung compliance due to progressive atelectasis and air trapping, significantly increasing breathing work, cardiovascular dysfunction, causes of cardiorespiratory morbidity, and mortality.⁵⁻⁷

MFS exhibits considerable phenotypic variation, including within families that carry the same genetic mutation.⁸ Numerous patient characteristics have been explored to explicate the significant phenotypic variation observed in MFS.⁹ A diverse array of mutation types and sites in the *FBN1* gene has been linked to disease severity and response to pharmaceutical interventions.⁹⁻¹³ Reduced expression of the wildtype *FBN1* allele has been implicated in contributing to disease severity.¹⁴ In addition, altered expression patterns of *FBN1* transcript isoforms were identified in MFS patients relative to unaffected individuals.¹⁵ Furthermore, genetic variants in other genes at distinct chromosomal regions, such as *COL4A1* and *PRKG1*, have been linked to exacerbating aortic pathology in MFS, thereby implying the involvement of potential pathogenic genes beyond *FBN1*.¹⁶

Recent research has demonstrated that DNA hypomethylation patterns within the CpG island shores of the *FBN1* gene are linked to differential expression levels of *FBN1* in porcine liver and fetal fibroblasts, thus suggesting its role in regulating tissue/cell type-specific gene expression.¹⁷ Moreover, hypermethylation of the *FBN1* gene has been identified as a potential biomarker for multiple cancers in various patient groups.¹⁸⁻²⁰ Notably, Arai et al.²¹ proposed a possible link between DNA methylation ambiguity within the CpG island shore of *FBN1* and *FBN1* mRNA levels, thus suggesting its involvement in MFS. However, an epigenome-wide association study (EWAS) did not detect any methylation sites near the *FBN1* gene that were linked to the MFS phenotype.⁸ Instead, the study found several other methylation loci significantly associated with aortic dimensions, aortic dilation rate, and aortic events in patients with MFS. Nevertheless, differentially methylated positions (DMPs) associated with scoliosis of MFS is not fully investigated.

This report evaluates DNA methylation and transcription profiles from whole blood in MFS with scoliosis required spinal deformity correction. We hypothesized that DNA methylation levels would:

(1) correlate with the specificity of organ involvement especially spinal deformity in MFS, (2) reflect the severity of MFS, and (3) regulate gene expression.

2 | MATERIALS AND METHODS

2.1 | Patients and controls enrollment

The procedures involving human participants in this study were ethically reviewed and approved by the Institutional Ethics Review Board of the Second Xiangya Hospital, People's Republic of China. All individual participants included in the study provided informed consent. The cohort comprised seven patients who required spinal deformity correction, and they were clinically diagnosed with classical MFS based on the current Ghent nosology.²² In order to exclude any potential cardiac or extracardiac abnormalities, all healthy controls (HCs) underwent a physical examination, which included measuring blood pressure and transcutaneous oxygen saturation. Additionally, full-length spine X-ray shows no spinal deformity and none of them exhibited any heart dysfunction on the echocardiogram.

2.2 | Sample collection

Whole blood samples were collected from all participants between 8:00 and 11:00 am following an overnight fast. PAXgene blood tubes and EDTA tubes were used for blood collection. After collecting whole blood samples in PAXgene blood tubes, the specimens were allowed to incubate at room temperature for a period of 2 h. This step was carried out to ensure complete lysis of blood cells and optimize RNA preservation in the samples. The tubes were subsequently stored at a temperature of -20°C until RNA isolation was performed.

2.3 | Illumina 850K (EPIC) DNA methylation array

Total DNA was isolated and purified using the DNeasy Blood Kit (Cat#69504, QIAGEN, Germany). Bisulfite conversion of the blood DNA was carried out using the EZ DNA Methylation-Gold™ Kit (D5005, Zymo, USA). To determine the overall DNA methylation status of 12 specimens under investigation, we used the Illumina Infinium Methylation EPIC 850K BeadChip, which provided high-throughput profiling of CpG methylation at single-nucleotide resolution. All discovery-phase samples were subjected to rigorous quality control tests before being analyzed using the Infinium® MethylationEPIC BeadChip (Illumina, San Diego, CA) following the manufacturer's instructions at Shanghai Biotechnology Corporation. The methylation level was scored based on β values ranging from 0 (unmethylated) to 1 (fully methylated). Probes containing single-nucleotide polymorphisms and probes located on the sex chromosome were initially excluded. Subsequent quality control and normalization of raw data

were performed using the bio-conductor R package minfi (v1.18.6). Imputation and normalization were subsequently carried out using the K-nearest neighbor method and the Subset-quantile Within Array Normalization (SWAN) algorithm Beta Mixture Quantile dilation methods, respectively. A threshold value of 0.1 for the delta β was used for filtration, with a p -value of 0.05.

2.4 | Functional enrichment analysis of differentially methylated genes

Gene Ontology analysis was carried out using Metascape²³ with default parameters. The Metascape software can be accessed freely at <https://metascape.org>. Before visualization, the observed gene count was transformed into a gene ratio (number of observed/total number of genes in a specific term). For visualization, the top 20 significant GO terms were chosen and ordered by utilizing hierarchical clustering on the distance of $-\log_{10} p$ -value.

2.5 | Enrichment analysis of differentially methylated genes in DisGeNET

The DisGeNET database combines multiple disease gene databases and is utilized to investigate disease-related genes.²⁴ We used Metascape, an online tool that includes multiple enrichment methods, to query DisGeNET and determine the proportion of genes enriched in MFS-related phenotypes.²³

2.6 | Correlation analysis

The severity of scoliosis was quantified using the Cobb angle method to assess the major curvature (Figure 4D)²⁵ by full-length spine x-ray. The Cobb angle was defined as the angle between the superior endplate of the upper vertebrae and the inferior endplate of the lower vertebrae. Vital capacity was evaluated following the recommendations of the Thoracic Society/European Respiratory Society,²⁶ and the percentage of predicted values (% predicted) for FEV1 was calculated. All methods were performed in accordance with approved guidelines and regulations. Correlations between DNA methylation and the Cobb angle of scoliosis and FEV1% predicted were assessed using Spearman's correlation coefficient.

2.7 | Protein–protein interaction networks construction and hub gene identification

The STRING database (version 11) which contains all known and protein–protein interaction (PPI) networks,²⁷ was utilized to investigate functional interactions between proteins. PPI networks of differentially methylated genes (DMGs) were constructed based on the STRING online tool. Following the removal of unconnected nodes

from the network, DMGs PPIs were visualized using Cytoscape (version 3.7.2). The CytoNCA plug-in of Cytoscape was applied to calculate degree centrality, betweenness centrality, and closeness centrality.

2.8 | Transcriptome sequencing

RNA-sequencing (RNA-seq) analysis of whole blood was performed by Shanghai Biotechnology Corporation (Shanghai, China). Total RNA was extracted from our samples using the RNeasy Mini Kit (Qiagen, Germany), which ensured high-quality RNA isolation. Paired-end libraries were constructed using the TruSeq™ RNA Sample Preparation Kit (Illumina, USA), according to the manufacturer's instructions. Poly-A-containing mRNA molecules were initially purified using poly-T oligo-attached magnetic beads, followed by fragmentation into smaller pieces using divalent cations under 94°C for 8 min. The cleaved RNA fragments were then converted into first-strand cDNA with random primers and reverse transcriptase, while second-strand cDNA synthesis was carried out using DNA polymerase I and RNase H. The resulting cDNA fragments underwent an end repair process, had a single “A” base added to each of them, and were ligated with adapters. After purification and PCR enrichment, the final cDNA library was created. The purified libraries were quantified using the Qubit® 2.0 fluorometer (Thermo Scientific, USA) and validated with the Agilent 2100 Bioanalyzer (Agilent Technologies, USA) to confirm insert size and calculate mole concentration. Cluster generation was achieved using cBot with the library diluted to 10 pM, and sequencing was carried out on the Illumina NovaSeq6000 (Illumina, USA), delivering high-throughput sequencing data of exceptional quality. To quantify gene expression levels in each sample, we calculated the fragments per kilobase per million mapped fragments (FPKM) value for each gene. Differential expression analysis was then performed using the edgeR package.²⁸ The threshold of different expression genes (DEGs) screening was set as follows: Fold-change ≥ 2 and p -value ≤ 0.05 .

2.9 | The weighted gene co-expression network analysis

The weighted gene co-expression network analysis (WGCNA) R package was utilized to identify co-expression modules from the entire transcript dataset.²⁹ The soft-thresholding power was set to 5 to optimize model fit using a scale-free topology approach. A dynamic tree-cutting algorithm with a minimum module size of 100 was used to determine initial module assignments. To summarize the transcription profile of each module, we calculated its first principal component (the module eigengene). Module eigengenes were subsequently analyzed for correlation with methylation-regulated DEGs (MeDEGs). Modules with the highest correlation coefficient with MeDEGs were labeled as hub modules to annotate the function of MeDEGs.³⁰

2.10 | Statistical analysis

Statistical significance of two independent groups was determined using Student's *t*-test. The correlation between differentially expressed genes and methylation levels was evaluated using Spearman's correlation coefficient. In both cases, statistical significance was established at $p < 0.05$. All statistical analyses were carried out using R 4.0.0.

3 | RESULTS

3.1 | Genome-wide DNA methylation profiles

All MFS patients presented with scoliosis requiring spinal correction, and the phenotype of MFS in our study was demonstrated in Figure 1A. An overview of the study design is illustrated in Figure 1B. The corresponding Manhattan plot highlighted that these DNA methylation sites were distributed across the genome (Figure 2A). PCA analysis revealed apparent methylation differences between MFS patients and HCs (Figure 2B). Using p -value < 0.05 and β difference ≥ 0.1 criteria, we identified 1253 DMPs which allocated to 236 genes. Of these, 509 (40.6%) DMPs were hypermethylated and 744 (59.4%) were hypomethylated. The volcano map displayed the differential methylation positions (Figure 2C). As indicated in Figure 2D,E, majority of differentially methylated probes located in the gene body, with 34% hypermethylated and 40% hypomethylated. Additionally, CpG island-based regions of significantly hypermethylated or hypomethylated CpG sites were dispersed in CpG islands (Figure 2D,E).

3.2 | Identification of MFS phenotype-related DMPs and hub genes analysis

To determine the general diseases associated with the 236 DMGs, we utilized gene ontology databases and publicly available metascape.org tool for pooling the DisGeNET database (Figure 3A).²⁴ Interestingly, the enriched terms were closely related to MFS phenotypes such as scoliosis, cardiomyopathy, and vital capacity, which contained 64 DMPs annotated to 44 DMGs, 66 DMPs annotated to 42 DMGs, and 38 DMPs annotated to 27 DMGs, respectively. We then screened out the DMGs enriched in these three MFS-associated phenotypes and conducted an analysis of PPI network using the STRING database, which was imported into Cytoscape for evaluating interactive relationships between candidate genes. The topological parameters of nodes based on degree, betweenness, and closeness were calculated using the CytoNCA plugin of the Cytoscape software. For scoliosis, TLE1 (cg14095100, cg20926353), PLXNA2 (cg10587082), CSMD1 (cg00259849), PAX3 (cg04302623), and FBXW7 (cg17682313) were the top five genes with high betweenness centrality (Figure 3B).

3.3 | Correlations between phenotype-related DMPs and clinical features of MFS

Among the DisGeNET enrichment of DMGs, scoliosis was the top two enrichments (Figure 3A), containing 64 DMPs. The differential methylation of these 64 DMPs was demonstrated in the cluster heat map (Figure 4A). Of these, 31 (48.4%) were hypermethylated, while 33 (51.6%) were hypomethylated. Most of the 64 DMPs are located in the gene body (72%), followed by 5'-UTR (16%; Figure 4B).

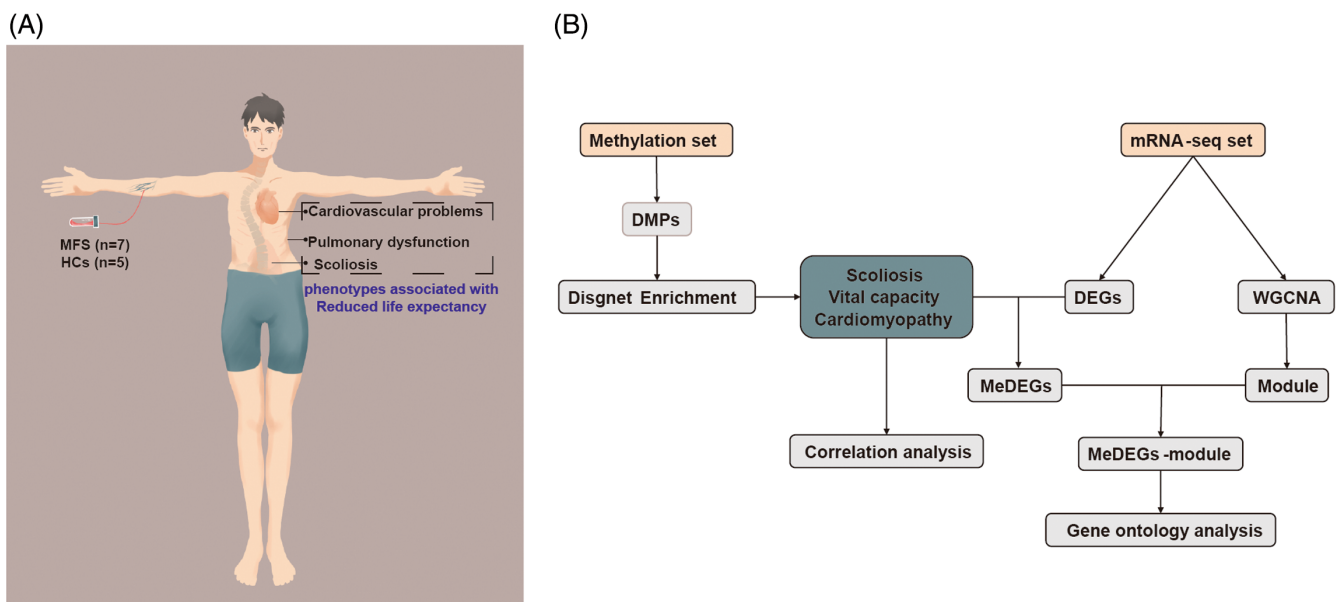


FIGURE 1 Overview of the study. (A) Patients included and phenotypes of MFS in our study. (B) Flowchart of bioinformatics analysis we conducted. DEGs, differentially expressed genes; DMGs, differentially methylated genes; DMPs, differentially methylated positions; HCs, healthy controls; MeDEGs, differentially methylated DEGs; MFS, Marfan syndrome.

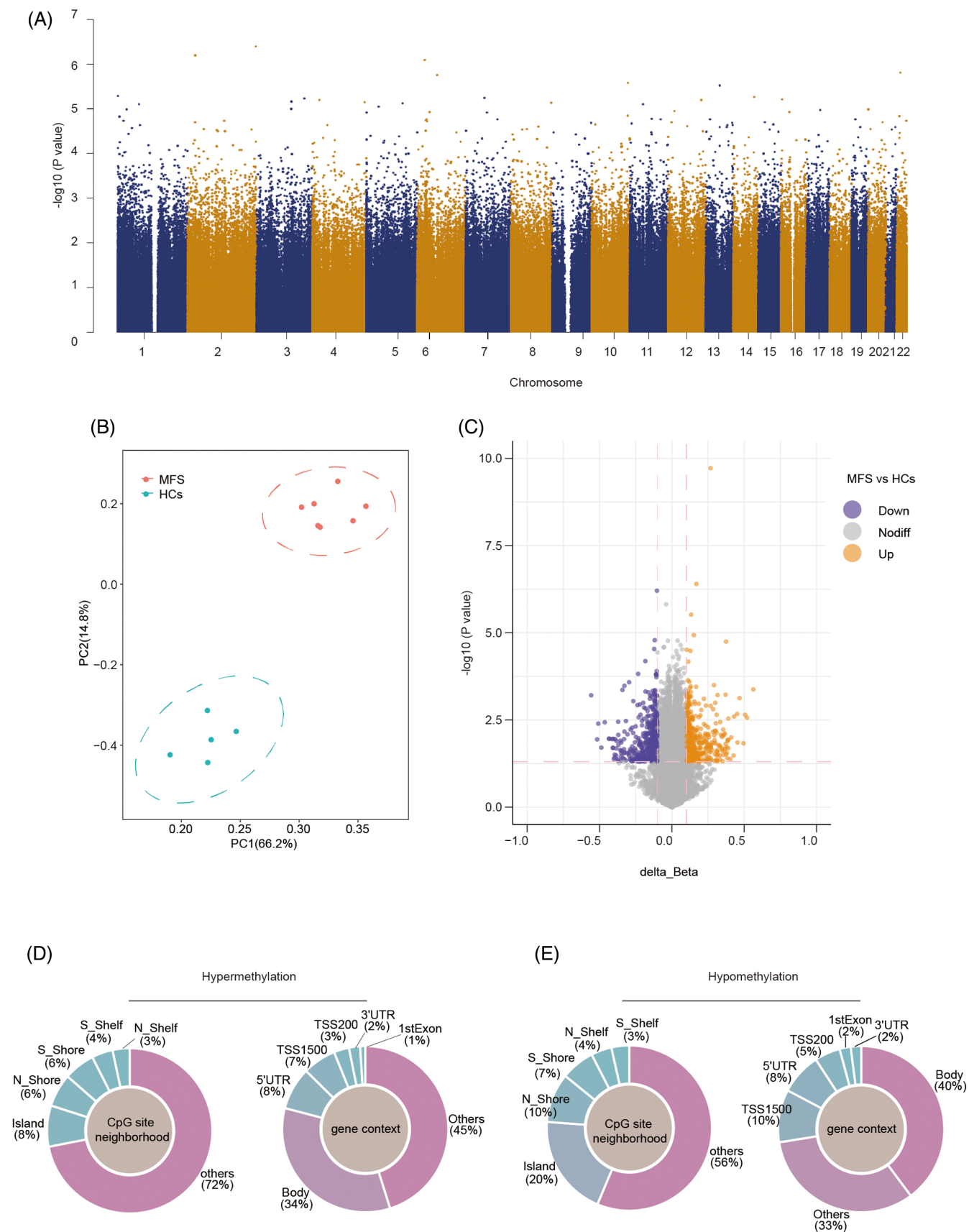


FIGURE 2 Identification of DNA methylation differences between MFS and HCs. (A) Manhattan plot showing chromosomal locations of $-\log_{10}(p \text{ values})$ for the difference at each locus in autosome. (B) PCA plot for divergent autosomal CpG methylation values. (C) Volcano plot of the differential methylation analysis showing 1253 DMPs. Vertical dotted lines: $\Delta\beta \geq 0.1$ or ≤ -0.1 ; Horizontal dotted line: the significance cutoff ($p\text{-value} = 0.05$). (D, E) The genomic distribution of differentially methylated probes in the gene context and CpG-island neighborhood. DMPs, differentially methylated positions; HCs, healthy controls; MFS, Marfan syndrome; PCA, principal component analysis; TSS, transcription start site; UTR, untranslated region.

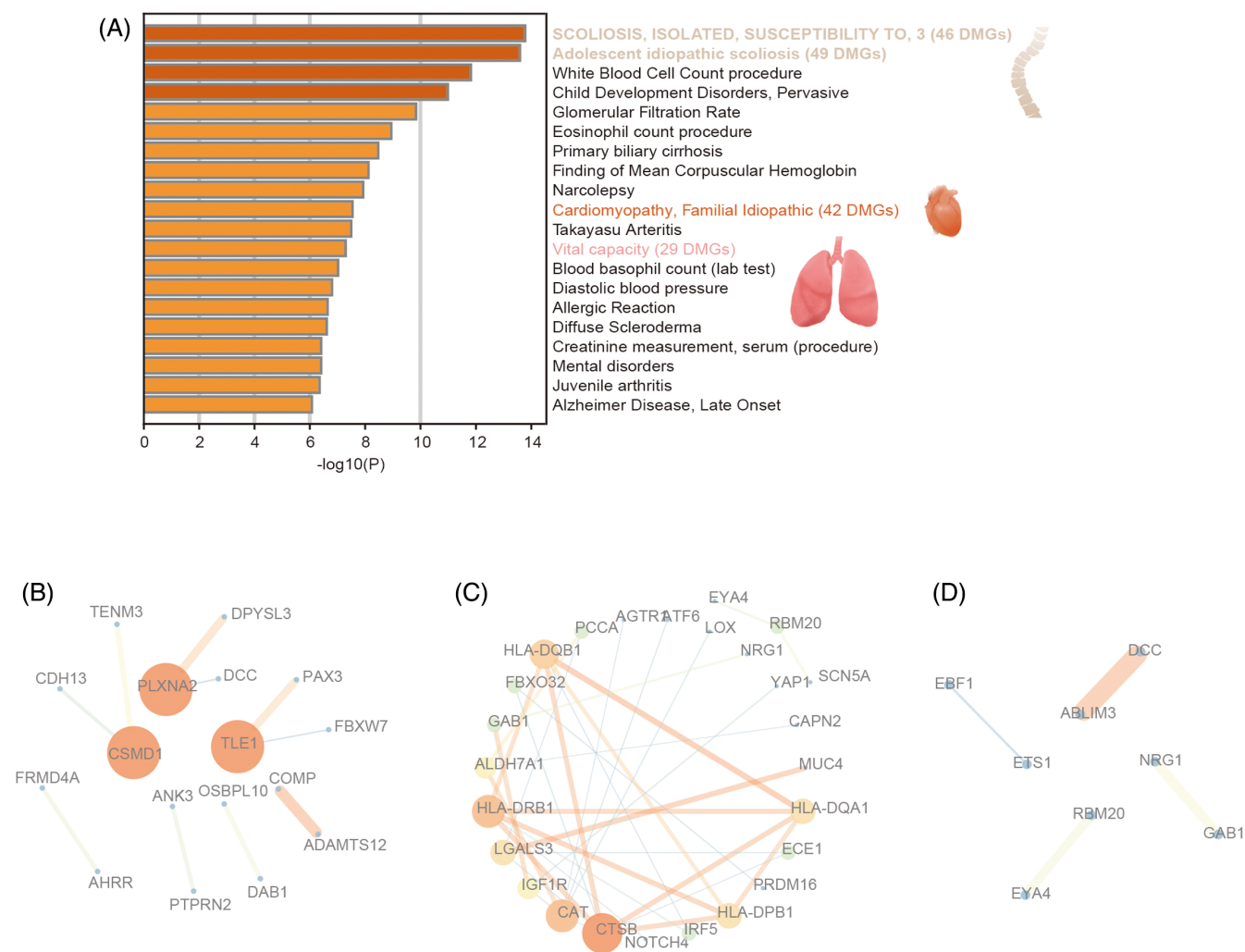


FIGURE 3 Identification of MFS phenotype-related DMGs. (A) Summary of 236 DMGs (1253 DMPs) enrichment analysis based on DisGeNET database. (B) Hub genes analysis of 49 DMGs (64 DMPs) enriched in scoliosis by the PPI network. (C) Hub genes analysis of 42 DMGs (66 DMPs) enriched in cardiomyopathy by the PPI networks. (D) Hub genes analysis of 29 DMGs (38 DMPs) enriched in vital capacity by the PPI network. DMGs, differentially methylated genes; DMPs, differentially methylated positions; PPI, protein-protein interaction.

Additionally, 12% were enriched within CpG islands (Figure 4C). Correlation analysis revealed a significant relationship between the Cobb angle (Figure 4D) and methylation state of multiple CpG sites. The top five Spearman's correlation coefficients are shown in Figure 4E-I.

Cardiomyopathy-associated DMPs containing 66 CpG sites (Figure 5A). Among these, 22 (33.3%) were hypermethylated, while 44 (66.7%) were hypomethylated. Most of the 66 DMPs are located in the gene body (55%), followed by TSS200 and TS1500 (13%; Figure 5B). Additionally, 18% were enriched within CpG islands (Figure 5C). Among the MFS patients included in our study, three had received cardiovascular surgery. We further compared the different methylation levels between patients with the history of cardiac surgery and no history of cardiac surgery in the 66 DMPs. Three DMPs showed significant differences between the two groups: cg00598125 (HLA-DRB1), cg24359717 (FBXO32), and cg27107292 (HLA-DRB1; Figure 5D-F).

The DisGeNET enrichment (Figure 6A) identified 38 DMPs associated with vital capacity, with 15 (39.5%) being hypermethylated and 23 (60.5%) being hypomethylated. The majority of the 38 DMPs are located in the gene body (76%), followed by 1stExon (11%; Figure 6B). Additionally, 18% were enriched within CpG islands (Figure 6C). Correlation analysis revealed a significant relationship between the GOLD grade of FEV1% predicted (Figure 6D-H) and methylation state of multiple CpG sites. The Spearman's correlation coefficients of the top 5 relationships are depicted in Figure 6D-H.

3.4 | Integrative analysis of gene expression and methylation

Our transcriptome sequencing data demonstrated obvious differences between MFS patients and HCs, as shown by PCA analysis (Figure 7A). Utilizing only differentially expressed transcripts with a

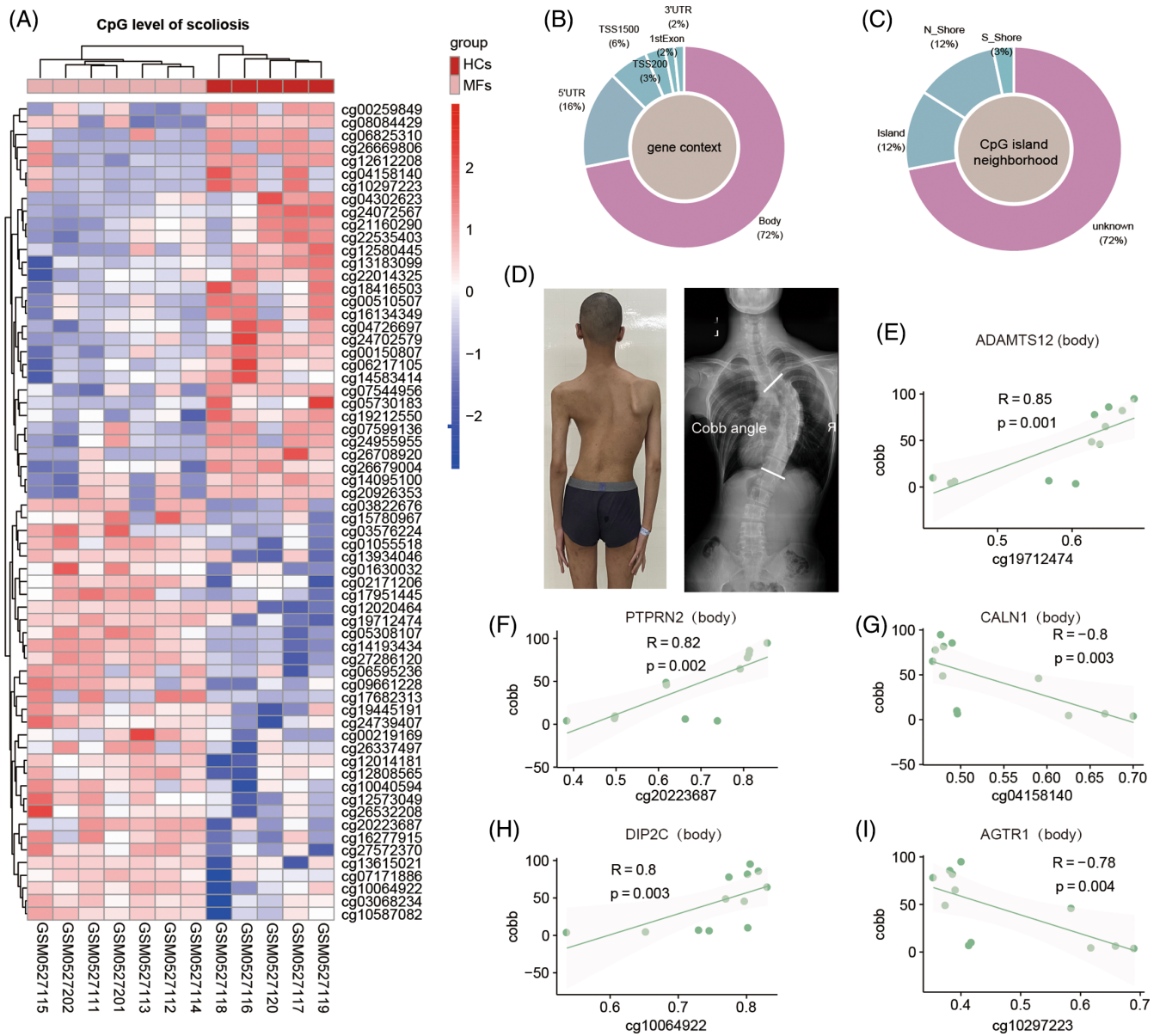


FIGURE 4 Analysis of scoliosis-related DMPs. (A) Heatmap of methylation changes at the 64 DMPs. (B, C) The genomic distribution of DMPs in the gene context and the CpG-island neighborhood. (D) Representative images of an MFS patient with scoliosis in posteroanterior views and full-length spine x-ray showing a main curve using cobb angle measurement. (E–I) The top five Spearman's correlation coefficients between scoliosis-related DMPs and cobb angle of scoliosis. DMPs, differentially methylated positions; MFS, Marfan syndrome.

2-fold or greater change in MFS versus HCs, we identified a total of 734 transcripts, including 283 downregulated and 451 upregulated transcripts (p -value < 0.05, fold change ≥ 2) (Figure 7B). Intersection of DEGs and DMGs enriched in scoliosis generated MeDEGs, where four MeDEGs were obtained, such as PTPRN2, CSMD1, LINC01006, and SYCP2L (Figure 7C). All four DMPs were located in the gene body of MeDEGs (Figure 7D–G). Specifically, cg20223687 was hypermethylated and corresponded with upregulated PTPRN2; cg00259849 was hypomethylated and corresponded with upregulated CSMD1; cg24702579 was hypomethylated and corresponded with upregulated LINC01006; cg16277915 was hypermethylated and corresponded with downregulated SYCP2L. Furthermore, by intersecting the DEGs and DMGs enriched in cardiomyopathy, we identified two

MeDEGs: an increase in HLA-DRB1 and a decrease in IGF1R (Figure S1A,B). The corresponding DMPs for HLA-DRB1 are presented in Figure 5D,F. Additionally, hypermethylation of cg13297560 in the gene body of IGF1R is shown in Figure S1C. No MeDEGs were identified in relation to vital capacity in MFS.

3.5 | Identification of co-expression modules related to PTPRN2 associated with scoliosis defines a link to ERKs inactivation

To gain a systems-level understanding of the function of MFS scoliosis-related MeDEGs, we performed a WGCNA analysis to

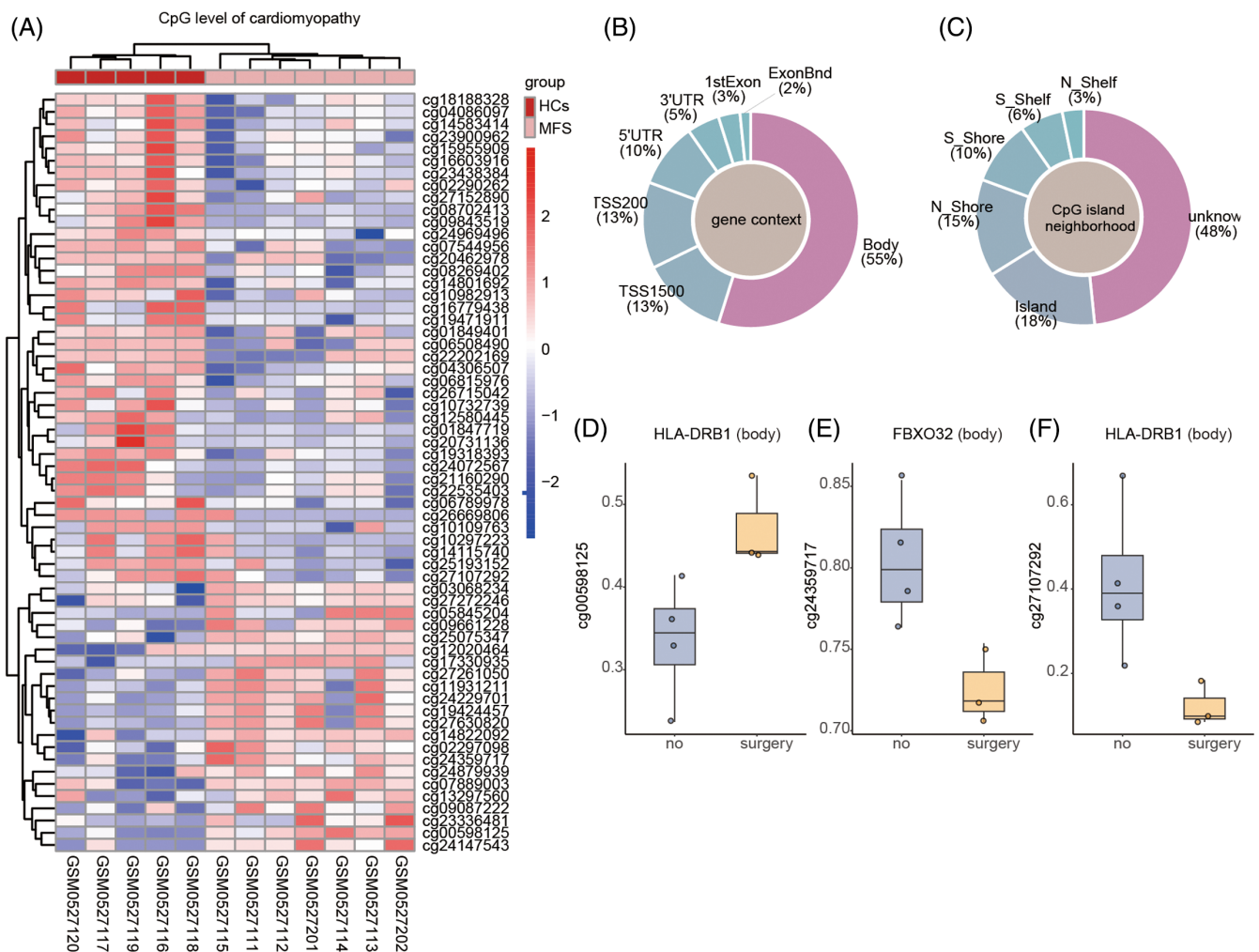


FIGURE 5 Analysis of cardiomyopathy-related DMPs. (A) Heatmap of methylation changes at the 66 DMPs. (B, C) The genomic distribution of differentially methylated probes in the gene context and CpG-island neighborhood. (D-F) 3 CpG sites were different between patients with the history of cardiac surgery and no history of cardiac surgery among the 66 DMPs. DMPs, differentially methylated positions; MFS, Marfan syndrome.

evaluate the potential regulatory effect of the four MeDEGs on scoliosis in MFS. We identified 17 co-methylation modules that could be described by module eigengenes (Figure 8A). The salmon module was significantly correlated with PTPRN2 ($R = 0.62$, $FDR = 0.03$). We further explore the function of salmon module genes by GO enrichment analysis using Metascape. This analysis identified multiple GO terms at an $FDR < 0.05$, and the top 20 terms were presented (Figure 8B). Notably, the salmon module exhibited enrichment in ERKs inactivation.

4 | DISCUSSION

The objective of this study was to investigate the heterogeneity of MFS phenotypes through an integrative analysis of DNA methylation and transcriptome data. Our results revealed that DNA methylation can effectively distinguish between MFS and HCs, with DMGs primarily enriched in scoliosis, cardiomyopathy, and vital capacity—conditions often associated with reduced lifespan in

untreated MFS. Further analysis unveiled a positive correlation between the upregulation of cg20223687 (PTPRN2) and the Cobb angle of scoliosis, suggesting its potential involvement in ERKs inactivation. Taken together, our findings have identified DNA methylation-regulated genes that may provide crucial insights into the biological mechanisms underlying MFS phenotypic regulation.

Cardiovascular dysfunction is a major cause of reduced lifespan and mortality of MFS patients.³¹ In a study conducted by Mitzi et al.,⁸ seven DMPs were identified that were associated with cardiovascular diseases and significantly linked to aortic diameters in MFS patients. Additionally, they found five DMPs (SAMD4A, IGF2BP3, PIP4K2A, BMP15, and HDAC4) that were linked to clinical events.⁸ In our study, we discovered 66 DMPs located within 42 genes, which were enriched in cardiomyopathy. Notably, three DMPs, annotated to HLA-DRB1 (cg00598125 and cg27107292), and FBXO32 (cg24359717), were associated with clinical events related to cardiac surgery. HLA-DRB1 belongs to the HLA class II beta chain paralogs and plays a crucial role in the immune system.^{32,33} Teodora et al.

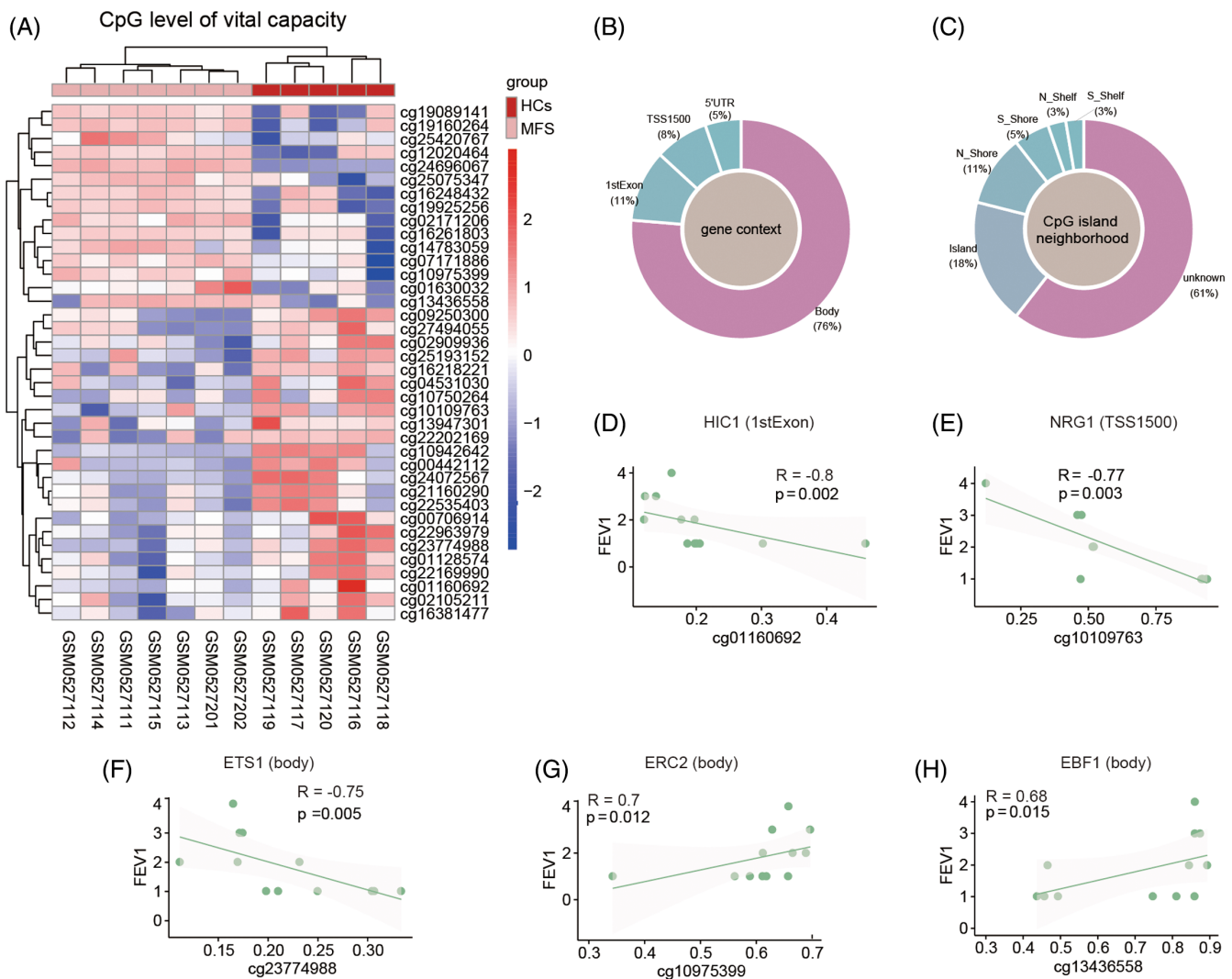


FIGURE 6 Analysis of vital capacity-related DMPs. (A) Heatmap of methylation changes at the 38 DMPs. (B, C) The genomic distribution of differentially methylated probes in the gene context and CpG-island neighborhood. (D–H) The top five Spearman's correlation coefficient between lung function-related DMPs and FEV1% were predicted. DMPs, differentially methylated positions.

demonstrated, through microarray data analysis, that increased expression of HLA-DRB1 was associated with key clinical features in MFS patients, including the severity of aortic root dilatation and specific skeletal abnormalities.³⁴ Furthermore, Deng revealed an association between HLA-DRB1 gene polymorphism and idiopathic dilated cardiomyopathy.³⁵ Our RNA-sequencing data, consistent with the findings of Teodora et al.,³⁴ also showed increased expression of HLA-DRB1 in MFS, suggesting its potential involvement in cardiovascular dysfunction in MFS. FBXO32 (MAFbx1/Atrogin1) is a muscle-specific F-Box protein with E3 ligase activity that specifically localizes at the sarcomere in the heart.³⁶ Although the DMP (cg24359717) in the body region of FBXO32 was associated with clinical events related to cardiac surgery, no significant difference in expression level was observed. Another DMG that was enriched in cardiomyopathy and showed differential expression in our study was IGF1R. The binding of IGF1R in the IGF-1 signaling pathway of smooth muscle cells and fibroblasts is crucial for normal vascular wall development.³⁷

Recently, IGF1R has been identified as a critical gene involved in aortic dissection.³⁸ These findings improve our understanding of the mechanisms underlying cardiovascular dysfunction in MFS patients.

Pulmonary involvement is observed in approximately 63% of MFS, and it is characterized by either restrictive or obstructive lung disease resulting from spinal deformities or abnormal lung parenchyma.^{39–43} In our study, we identified DMGs enriched in vital capacity, including 38 CpG sites. Among these, cg01160692 (HIC1), cg10109763 (NRG1), cg23774988 (ETS1), cg10975399 (ERC2), and cg13436558 (EBF1) showed the strongest association with FEV1% predicted. HIC1, a growth regulatory gene, has been linked to tumors and Miller–Dieker syndrome when hypermethylated or deleted in its genomic region.^{44,45} Furthermore, genetic variants (rs3803809) of HIC1 have shown an association with vital capacity.⁴⁶ In our study, we found hypermethylation of cg01160692 in the first exon of HIC1, which was associated with a lower vital capacity measured by FEV1% predicted. NRG1 encodes a membrane glycoprotein involved in

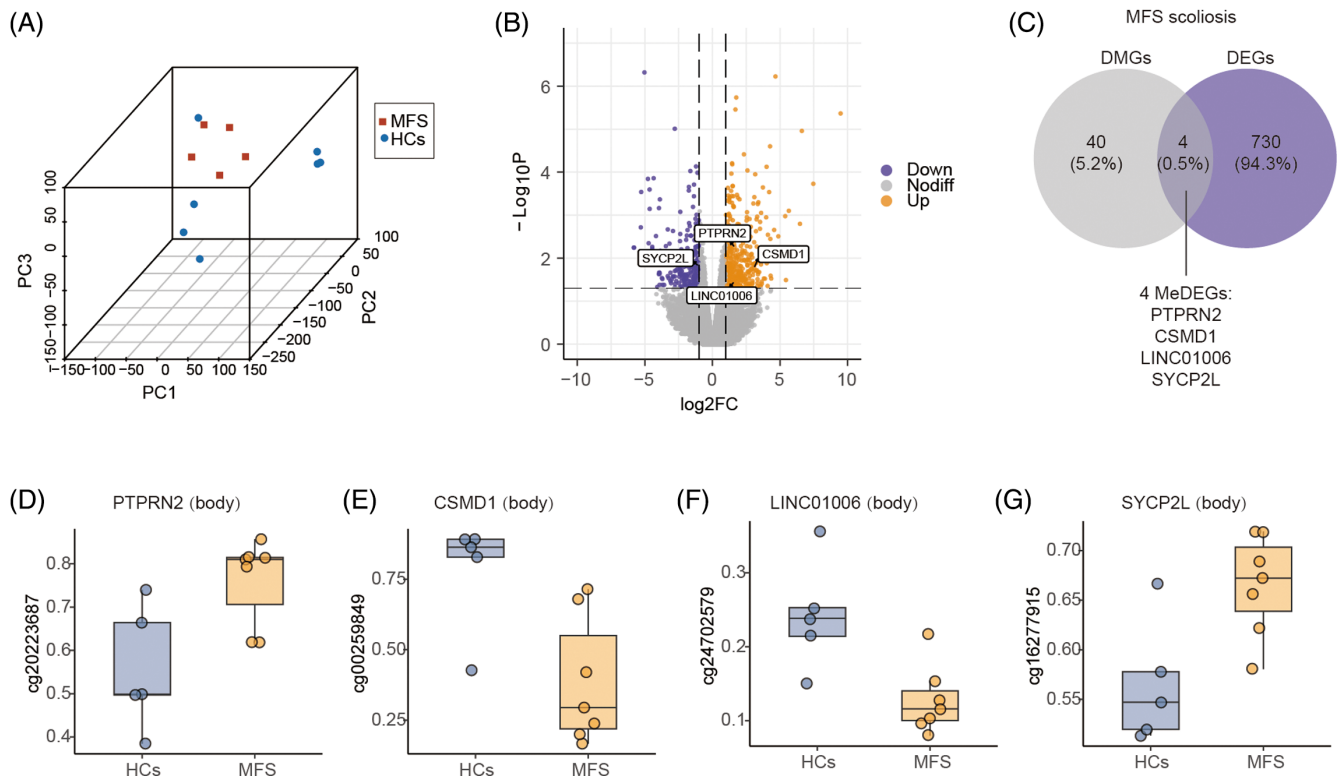


FIGURE 7 Differential transcriptome analysis. (A) 3D-PCA analysis. (B) The volcano plot of DEGs with 283 downregulated and 451 upregulated transcripts. Vertical dotted lines: $\text{Log}_2\text{FC} \geq 1$ or ≤ -1 ; Horizontal dotted line: the significance cutoff (p -value = 0.05). (C) Intersection of DEGs and DMGs enriched in MFS scoliosis generated four MeDEGs. (D–G) Boxplot displays the four DMPs in MeDEGs. 3D-PCA, three-dimensional principal component analysis; DEGs, differentially expressed genes; MeDEGs, methylation regulated DEGs.

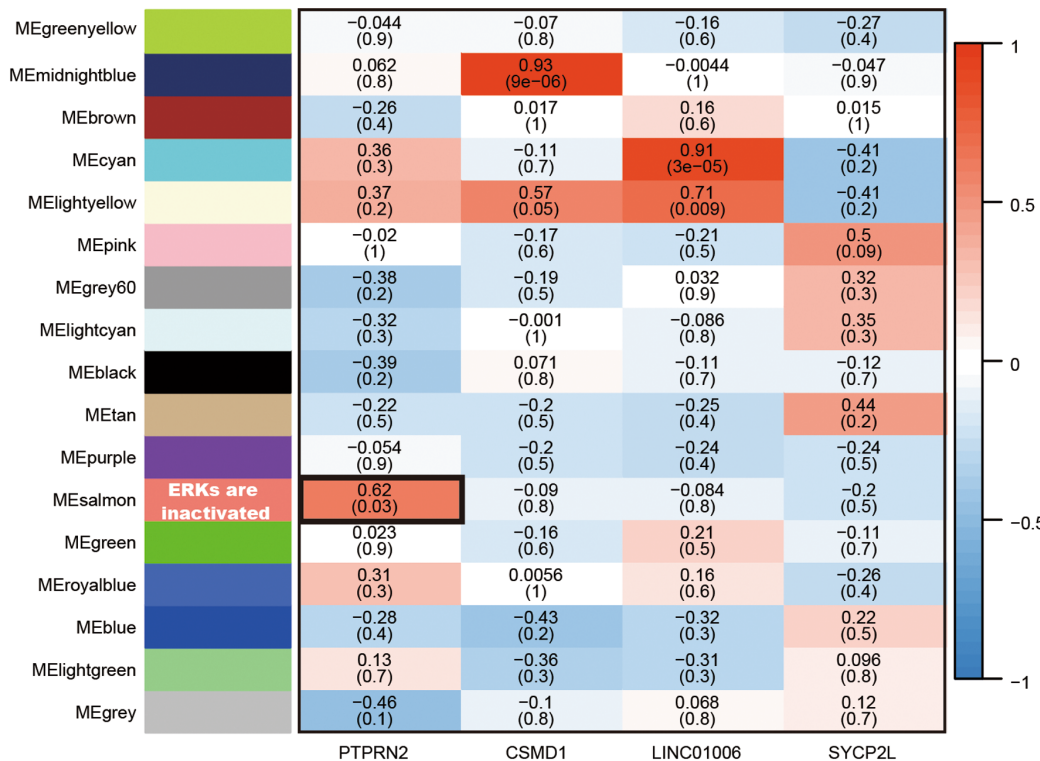
cell-cell signaling and plays a crucial role in multiple organ system growth and development.^{47–49} Previous studies have reported significant associations between *NRG1* gene variants (rs35033136 and rs7000590) and diffusing capacity of carbon monoxide in European ancestry white and African-American cohorts.⁵⁰ In our study, hypermethylation of cg10109763, located in the TSS1500 region of *NRG1*, was associated with a lower vital capacity. The *Ets* family of genes encodes transcription factors, among which *ETS1* is an early hypoxia-responsive gene highly expressed in organs undergoing branching morphogenesis, such as the lung.⁵¹ Reduced expression levels of *ETS1*, regulated by miRNA, have been linked to susceptibility to high-altitude pulmonary edema under hypobaric hypoxia conditions.⁵² In our study, we observed hypermethylation of cg23774988 in the body region of *ETS1*, which was associated with a lower vital capacity. *ERC2* encodes a protein belonging to the Rab3-interacting molecule (RIM)-binding protein family, involved in regulating neurotransmitter release at the cytomatrix in active zones (CAZ) complex.^{53,54} Genetic variants (rs4955883) of *ERC2* have shown an association with vital capacity.⁴⁶ In our study, hypermethylation of cg10975399 in the body region of *ERC2* was associated with a higher vital capacity measured by FEV1% predicted. *EBF1*+ fibroblasts have been suggested as potential progenitor cells of lung pericytes during early lung development.⁵⁵ These fibroblasts contribute to matrix deposition and are associated with invasive, proliferative, and contraction phenotypes

linked to progressive pulmonary fibrosis.⁵⁶ In our study, hypermethylation of cg13436558 in the body region of *EBF1* was associated with a higher vital capacity measured by FEV1% predicted. Despite abnormal methylation modifications, these genes showed unchanged gene expression. Further validation is needed, but these DMPs hold potential as biomarkers for assessing vital capacity in MFS patients.

Scoliosis is a prevalent spinal deformity in individuals with MFS, with reported prevalence ranging from 52% to 100%.^{57,58} Rapid aggravation of scoliosis tends to occur during infancy and adolescence, which coincide with periods of rapid height growth.^{59–62} Individuals with untreated scoliosis, particularly those with severe cases, are at an increased life shortening and mortality.⁴ The higher mortality seen in individuals with untreated severe scoliosis can be attributed to structural changes that impede the thoracic cavity, resulting in restrictive lung disease, cardiovascular complications, and respiratory failure.^{4,63–65} Both genetics and epigenetics play important roles in the occurrence and development of scoliosis.⁶⁶ Genome-wide association studies (GWAS) have been valuable for identifying genetic variants associated with scoliosis as a polygenic disease, such as *TLE1*, *PLXNA2*, *PAX3*, *FBXW7*, and *CSMD1*. These genes exhibited the highest degrees of association in the PPI analysis conducted on the DMGs associated with scoliosis in our study. The *TLE1* gene variant (rs11139357) has been implicated in congenital scoliosis,⁶⁷ while *PLXNA2* gene variants (rs17011903 for adolescent idiopathic

(A)

Module-MeDEGs relationships



(B)

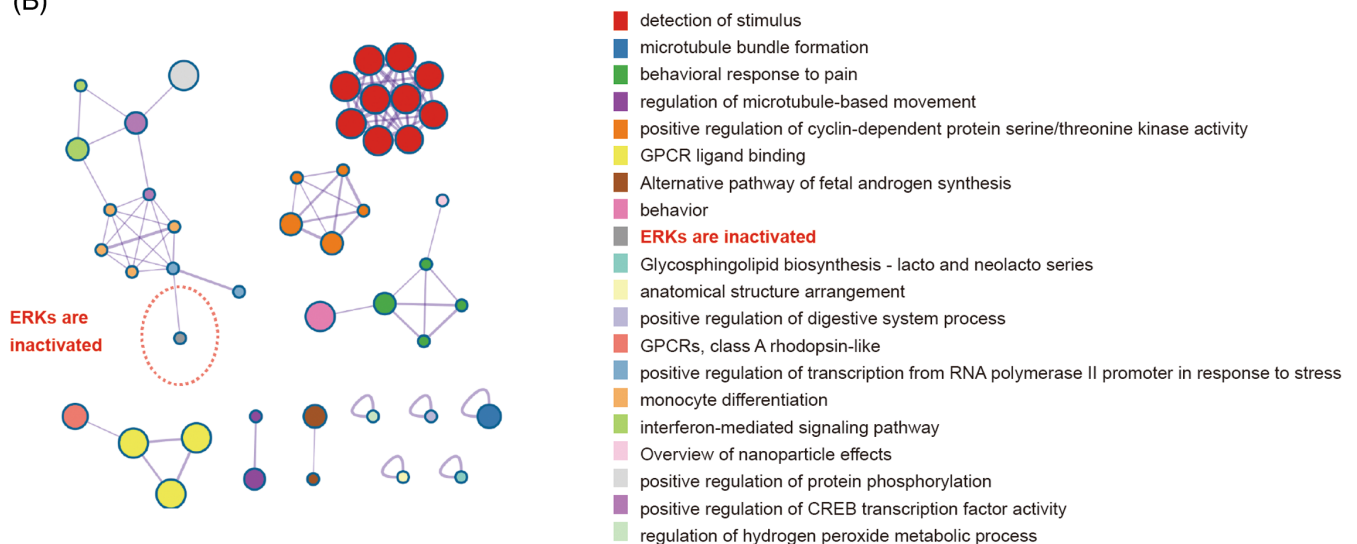


FIGURE 8 WGCNA was used to identify the hub module genes of the four MeDEGs associated with MFS scoliosis. The analysis revealed 17 gene modules (A) that were correlated with the four MeDEGs. The hub modules, which exhibited the strongest correlation with PTPRN2 and a p -value < 0.05 , were selected for further investigation. Among these, the salmon module displayed a significant correlation with PTPRN2 ($R = 0.62$, $FDR = 0.03$). To gain insight into the gene functions of PTPRN2 in MFS scoliosis, functional enrichment analyses were conducted on the hub module genes of the salmon module. (B) The top 20 GO terms were enriched in the salmon gene modules. Notably, the salmon module exhibited significant enrichment for ERKs inactivation, thus suggesting potential biological functions for this module that are further highlighted in Figure 8A. GO, Gene Ontology; MeDEGs, methylation regulated differentially expressed genes; MFS, Marfan syndrome; WGCNA, weighted gene correlation network analysis.

scoliosis⁶⁸ and rs7516841 for congenital scoliosis⁶⁷) have been identified. Abnormal expression of PAX3 has been associated with anomalous paravertebral muscle development in adolescent idiopathic

scoliosis.⁶⁹ Furthermore, a significant association has been reported between the FBXW7 gene variant (rs4315757) and congenital scoliosis.⁶⁷ CSMD1, encoding a complement control protein involved in

complement activation and inflammation in the developing central nervous system, has been associated with scoliosis risk. The CSMD1 gene variants (rs11136775 and rs13260434) have shown associations with congenital scoliosis,⁶⁷ and rs11787412 has been linked to adolescent idiopathic scoliosis.⁶⁸ Notably, CSMD1 showed increased expression in our study. Associations have also been observed between the PAX3 gene variant (rs16863633) and both congenital and adolescent idiopathic scoliosis.⁶⁸ Emerging evidence suggests that epigenetics may play a role in the development and progression of non-Marfan syndrome scoliosis.^{66,70,71} Specifically, Meng et al.⁷² have identified hypomethylation of the cg01374129 site, which is associated with hyaluronan synthase 2 (HAS2), as a potential independent predictor for high-risk curve progression in scoliosis. These genetic variants at specific gene loci, along with DNA methylation modifications, may collectively regulate the development of spinal curvature.

Besides CSMD1, other DMGs linked to scoliosis, namely LINC01006, SYCP2L, and PTPRN2, exhibited distinct expression patterns in individuals with MFS. LINC01006 belongs to the long non-coding RNA (lncRNA) class and increased LINC01006 expression profiles related to apoptosis and autophagy in peripheral blood mononuclear cells of patients with rheumatoid arthritis.⁷³ A significant association has been reported between the LINC01006 gene variant (rs2140629) and scoliosis.⁶⁷ In our study, we observed an increase in the expression of LINC01006 in the MFS group. SYCP2L was predicted to be involved in meiotic nuclear division and accelerated reproductive aging has been observed in females who lack the presence of a novel centromere protein known as SYCP2L.⁷⁴ Previous research has shown associations between the SYCP2L gene variant (rs1225764) and adolescent idiopathic scoliosis.⁶⁷ In our study, we found a decrease in SYCP2L expression among MFS patients, suggesting a potential involvement of SYCP2L in MFS scoliosis.

In MFS-associated scoliosis, PTPRN2 demonstrated increased hypermethylation of cg20223687 in the gene body and upregulation of PTPRN2 transcription. A growing body of evidence indicates that gene body methylation can play a positive role in transcription by ensuring correct splicing and translation, suppressing spurious gene transcription, regulating alternative splicing, and promoting stable and ordered transcription.²⁰ In addition, cg20223687 exhibits a positive correlation with the Cobb angle of the major curve. PTPRN2 is a member of the N-type family of PTP receptors, typically expressed in the nervous system and endocrine cells, and has been shown to play a role in regulating insulin secretion.^{75,76} In a study by Liu et al.,⁶⁷ two single-nucleotide polymorphisms (SNPs), rs7802459 and rs896773, located in PTPRN2 were found to be associated with congenital scoliosis. In individuals with MFS, Mitzi et al.⁸ found DMPs could be attributed to PTPRN2. Our study identified hypermethylation of cg20223687 and upregulation of PTPRN2 transcription in MFS-associated scoliosis. To further elucidate the potential role of PTPRN2 in this context, we performed WGCNA and selected the salmon module as the most relevant gene module with PTPRN2, which suggested that PTPRN2 may play a role in ERK inactivation. Notably, ERK signaling is essential for osteoblast and chondrocyte proliferation and differentiation,⁷⁷⁻⁷⁹ as we previously demonstrated

in adolescent idiopathic scoliosis.⁸⁰ It is worth noting that in a significant number of studies on Marfan-related aortic aneurysms, the ERK pathway is typically activated.⁸¹⁻⁸³ However, the role of the ERK pathway in the development of spinal curvature may differ. In our previous research, we identified mutations and functional deficiencies in AKAP2 that are associated with adolescent idiopathic scoliosis.^{80,84} By isolating primary chondrocytes from human growth plates, we discovered that AKAP2 can activate the ERK pathway and promote chondrocyte proliferation, enhance differentiation, and promote extracellular matrix (ECM) synthesis. The functional loss of the AKAP2 gene may lead to the inhibition of the ERK pathway, resulting in the occurrence of scoliosis. Therefore, we hypothesize that hypermethylation of cg20223687 in gene body could lead to increased PTPRN2 transcription, which may inhibit ERKs signaling pathway and contribute to the progression of MFS-associated scoliosis. Further cellular and animal experiments are required to validate these findings. Collectively, our findings provide new insights into the molecular mechanisms underlying MFS-associated spinal deformities and may offer promising avenues for developing more effective therapeutic interventions.

4.1 | Limitation

One potential limitation of our study is the use of whole-blood samples. Ideally, we would have preferred to analyze connective tissue, such as aortic, cartilage, or skin tissue, as DNA methylation is tissue-specific. However, peripheral blood is easily accessible and thought to represent a signature that is concordant with other tissue types.⁸⁵ Another limitation of our study is the relatively small sample size. Nevertheless, the patients we included displayed representative and typical clinical features. Future research will involve collecting more clinical samples for validation purposes.

5 | CONCLUSION

To summarize, our study is the first to reveal that differential methylation sites are primarily enriched in phenotypes associated with reduced life expectancy in MFS, potentially explaining its phenotypic heterogeneity. While our findings provide new evidence concerning epigenetic imbalances and gene dysregulation in MFS scoliosis, additional mechanistic studies are necessary to fully comprehend how these epigenetic changes contribute to the observed phenotypes.

AUTHOR CONTRIBUTIONS

Zhen-zhong Zheng: Methodology, Data curation, Writing Original draft; **Jing-hong Xu:** Data collection; **Jia-lin Chen:** Data collection; **Bin Jiang:** Formal analysis; **Hong Ma:** Formal analysis; **Lei Li:** Critical revision of the manuscript for important intellectual content; **Ya-wei Li:** Project administration; **Yu-liang Dai:** Conceived of the study, and participated in its design and coordination; **Bing Wang:** Design, conceptualization, and helped to draft the manuscript. All authors read and approved the final manuscript.

ACKNOWLEDGMENTS

We thank all participating subjects for their kind cooperation in this study. We thank Professor Ming Zhao for discussions and helpful suggestions. We thank Dr Jianming Zeng (University of Macau), and all the members of his bioinformatics team, biotrainee, for generously sharing their experience and codes.

FUNDING INFORMATION

This work was supported by Hunan Provincial Key Research and Development Program (2021SK2002) and Hunan Province Science Foundation of China (2021JJ30938).

CONFLICT OF INTEREST STATEMENT

The authors declare that the research was conducted in the absence of any commercial or financial relationships that could be construed as a potential conflict of interest.

DATA AVAILABILITY STATEMENT

The datasets used and/or analyzed during the current study are available from the corresponding author upon reasonable request.

CONSENT FOR PUBLICATION

The informed consent has been obtained from all patients whose data are included in the publication.

ORCID

Bing Wang  <https://orcid.org/0000-0002-9647-5275>

REFERENCES

- Wright IH, Gaylard DG. Marfan's syndrome. *Anaesthesia*. 1985;40(2):206.
- Dietz HC, Cutting GR, Pyeritz RE, et al. Marfan syndrome caused by a recurrent de novo missense mutation in the fibrillin gene. *Nature*. 1991;352(6333):337-339.
- Milewicz DM, Braverman AC, de Backer J, et al. Marfan syndrome. *Nat Rev Dis Primers*. 2021;7(1):64.
- Pehrsson K, Larsson S, Oden A, Nachemson A. Long-term follow-up of patients with untreated scoliosis. A study of mortality, causes of death, and symptoms. *Spine*. 1992;17(9):1091-1096.
- Ruiz G, Torres-Lugo NJ, Marrero-Ortiz P, Guzmán H, Olivella G, Ramírez N. Early-onset scoliosis: a narrative review. *EFORT Open Rev*. 2022;7(8):599-610.
- Lin Y, Shen J, Chen L, et al. Cardiopulmonary function in patients with congenital scoliosis: an observational study. *J Bone Joint Surg Am*. 2019;101(12):1109-1118.
- Cipriano GF, Peres PA, Cipriano G Jr, Arena R, Carvalho AC. Safety and cardiovascular behavior during pulmonary function in patients with Marfan syndrome. *Clin Genet*. 2010;78(1):57-65.
- van Andel MM, Groenink M, van den Berg MP, et al. Genome-wide methylation patterns in Marfan syndrome. *Clin Epigenetics*. 2021;13(1):217.
- Faivre L, Collod-Beroud G, Loeys BL, et al. Effect of mutation type and location on clinical outcome in 1,013 probands with Marfan syndrome or related phenotypes and FBN1 mutations: an international study. *Am J Hum Genet*. 2007;81(3):454-466.
- Franken R, Teixeira-Tura G, Brion M, et al. Relationship between fibrillin-1 genotype and severity of cardiovascular involvement in Marfan syndrome. *Heart*. 2017;103(22):1795-1799.
- Radke RM, Baumgartner H. Diagnosis and treatment of Marfan syndrome: an update. *Heart*. 2014;100(17):1382-1391.
- Franken R, den Hartog AW, Radonic T, et al. Beneficial outcome of losartan therapy depends on type of FBN1 mutation in Marfan syndrome. *Circ Cardiovasc Genet*. 2015;8(2):383-388.
- Arnaud P, Milleron O, Hanna N, et al. Clinical relevance of genotype-phenotype correlations beyond vascular events in a cohort study of 1500 Marfan syndrome patients with FBN1 pathogenic variants. *Genet Med*. 2021;23(7):1296-1304.
- Aubart M, Gross MS, Hanna N, et al. The clinical presentation of Marfan syndrome is modulated by expression of wild-type FBN1 allele. *Hum Mol Genet*. 2015;24(10):2764-2770.
- Benarroch L, Aubart M, Gross MS, et al. Reference expression profile of three FBN1 transcript isoforms and their association with clinical variability in Marfan syndrome. *Genes*. 2019;10(2):128.
- Aubart M, Gazal S, Arnaud P, et al. Association of modifiers and other genetic factors explain Marfan syndrome clinical variability. *Eur J Hum Genet*. 2018;26(12):1759-1772.
- Arai Y, Umeyama K, Takeuchi K, et al. Establishment of DNA methylation patterns of the Fibrillin1 (FBN1) gene in porcine embryos and tissues. *J Reprod Dev*. 2017;63(2):157-165.
- Sharma P, Bhunia S, Poojary SS, et al. Global methylation profiling to identify epigenetic signature of gallbladder cancer and gallstone disease. *Tumour Biol*. 2016;37(11):14687-14699.
- Li WH, Zhang H, Guo Q, et al. Detection of SNCA and FBN1 methylation in the stool as a biomarker for colorectal cancer. *Dis Markers*. 2015;2015:657570.
- Koroknai V, Szász I, Hernandez-Vargas H, et al. DNA hypermethylation is associated with invasive phenotype of malignant melanoma. *Exp Dermatol*. 2020;29(1):39-50.
- Arai Y, Umeyama K, Okazaki N, et al. DNA methylation ambiguity in the fibrillin-1 (FBN1) CpG Island shore possibly involved in Marfan syndrome. *Sci Rep*. 2020;10(1):5287.
- von Kodolitsch Y, de Backer J, Schüller H, et al. Perspectives on the revised Ghent criteria for the diagnosis of Marfan syndrome. *Appl Clin Genet*. 2015;8:137-155.
- Zhou Y, Zhou B, Pache L, et al. Metascape provides a biologist-oriented resource for the analysis of systems-level datasets. *Nat Commun*. 2019;10(1):1523.
- Piñero J, Bravo À, Queralt-Rosinach N, et al. DisGeNET: a comprehensive platform integrating information on human disease-associated genes and variants. *Nucleic Acids Res*. 2017;45(D1):D833-d839.
- Cheung J, Wever DJ, Veldhuizen AG, et al. The reliability of quantitative analysis on digital images of the scoliotic spine. *Eur Spine J*. 2002;11(6):535-542.
- Miller MR, Hankinson J, Brusasco V, et al. Standardisation of spirometry. *Eur Respir J*. 2005;26(2):319-338.
- Szklarczyk D, Morris JH, Cook H, et al. The STRING database in 2017: quality-controlled protein-protein association networks, made broadly accessible. *Nucleic Acids Res*. 2017;45(D1):D362-D368.
- Robinson MD, McCarthy DJ, Smyth GK. edgeR: a Bioconductor package for differential expression analysis of digital gene expression data. *Bioinformatics*. 2010;26(1):139-140.
- Langfelder P, Horvath S. WGCNA: an R package for weighted correlation network analysis. *BMC Bioinformatics*. 2008;9:559.
- Gomez JL, Chen A, Diaz MP, et al. A network of sputum MicroRNAs is associated with neutrophilic airway inflammation in asthma. *Am J Respir Crit Care Med*. 2020;202(1):51-64.
- Vanem TT, Geiran OR, Krohg-Sørensen K, Røe C, Paus B, Rand-Hendriksen S. Survival, causes of death, and cardiovascular events in patients with Marfan syndrome. *Mol Genet Genomic Med*. 2018;6(6):1114-1123.
- Lester DK, Burton C, Gardner A, et al. Fucosylation of HLA-DRB1 regulates CD4(+) T cell-mediated anti-melanoma immunity and enhances immunotherapy efficacy. *Nat Cancer*. 2023;4(2):222-239.

33. Ranasinghe S, Cutler S, Davis I, et al. Association of HLA-DRB1-restricted CD4⁺ T cell responses with HIV immune control. *Nat Med*. 2013;19(7):930-933.
34. Radonic T, de Witte P, Groenink M, et al. Inflammation aggravates disease severity in Marfan syndrome patients. *PLoS One*. 2012;7(3):e32963.
35. Deng J, Luo R, Li X. HLA-DRB1 gene polymorphism is associated with idiopathic dilated cardiomyopathy: a meta-analysis. *J Cardiovasc Med (Hagerstown)*. 2011;12(9):648-652.
36. Al-Yacoub N, Shaheen R, Awad SM, et al. FBXO32, encoding a member of the SCF complex, is mutated in dilated cardiomyopathy. *Genome Biol*. 2016;17:2.
37. Sukhanov S, Higashi Y, Shai SY, et al. SM22 α (smooth muscle protein 22- α) promoter-driven IGF1R (insulin-like growth factor 1 receptor) deficiency promotes atherosclerosis. *Arterioscler Thromb Vasc Biol*. 2018;38(10):2306-2317.
38. Zhang H, Bian C, Tu S, et al. Integrated analysis of lncRNA-miRNA-mRNA ceRNA network in human aortic dissection. *BMC Genomics*. 2021;22(1):724.
39. Giske L, Stanghelle JK, Rand-Hendrikssen S, Strøm V, Wilhelmsen JE, Røe C. Pulmonary function, working capacity and strength in young adults with Marfan syndrome. *J Rehabil Med*. 2003;35(5):221-228.
40. Dyhdalo K, Farver C. Pulmonary histologic changes in Marfan syndrome: a case series and literature review. *Am J Clin Pathol*. 2011;136(6):857-863.
41. Corsico AG, Grosso A, Tripon B, et al. Pulmonary involvement in patients with Marfan syndrome. *Panminerva Med*. 2014;56(2):177-182.
42. Otremski H, Widmann RF, di Maio MF, Ovadia D. The correlation between spinal and chest wall deformities and pulmonary function in Marfan syndrome. *J Child Orthop*. 2020;14(4):343-348.
43. Streeten EA, Murphy EA, Pyeritz RE. Pulmonary function in the Marfan syndrome. *Chest*. 1987;91(3):408-412.
44. Fleuriel C, Touka M, Boulay G, Guérardel C, Rood BR, Leprince D. HIC1 (hypermethylated in cancer 1) epigenetic silencing in tumors. *Int J Biochem Cell Biol*. 2009;41(1):26-33.
45. Dubuissez M, Faiderbe P, Pinte S, Dehennaut V, Rood BR, Leprince D. The reelin receptors ApoER2 and VLDLR are direct target genes of HIC1 (hypermethylated in cancer 1). *Biochem Biophys Res Commun*. 2013;440(3):424-430.
46. Kichaev G, Bhatia G, Loh PR, et al. Leveraging polygenic functional enrichment to improve GWAS power. *Am J Hum Genet*. 2019;104(1):65-75.
47. Burden S, Yarden Y. Neuregulins and their receptors: a versatile signaling module in organogenesis and oncogenesis. *Neuron*. 1997;18(6):847-855.
48. Ritch PS, Carroll SL, Sontheimer H. Neuregulin-1 enhances survival of human astrocytic glioma cells. *Glia*. 2005;51(3):217-228.
49. Bublil EM, Yarden Y. The EGF receptor family: spearheading a merger of signaling and therapeutics. *Curr Opin Cell Biol*. 2007;19(2):124-134.
50. Terzikhan N, Sun F, Verhamme FM, et al. Heritability and genome-wide association study of diffusing capacity of the lung. *Eur Respir J*. 2018;52(3):1800647.
51. Kola I, Brookes S, Green AR, et al. The Ets1 transcription factor is widely expressed during murine embryo development and is associated with mesodermal cells involved in morphogenetic processes such as organ formation. *Proc Natl Acad Sci USA*. 1993;90(16):7588-7592.
52. Alam P, Agarwal G, Kumar R, et al. Susceptibility to high-altitude pulmonary edema is associated with circulating miRNA levels under hypobaric hypoxia conditions. *Am J Physiol Lung Cell Mol Physiol*. 2020;319(2):L360-L368.
53. Kiyonaka S, Nakajima H, Takada Y, et al. Physical and functional interaction of the active zone protein CAST/ERC2 and the β -subunit of the voltage-dependent Ca(2+) channel. *J Biochem*. 2012;152(2):149-159.
54. Neumann A, Walton E, Alemany S, et al. Association between DNA methylation and ADHD symptoms from birth to school age: a prospective meta-analysis. *Transl Psychiatry*. 2020;10(1):398.
55. Liu X, Rowan SC, Liang J, et al. Categorization of lung mesenchymal cells in development and fibrosis. *iScience*. 2021;24(6):102551.
56. Liu X, Dai K, Zhang X, et al. Multiple fibroblast subtypes contribute to matrix deposition in pulmonary fibrosis. *Am J Respir Cell Mol Biol*. 2023;69(1):45-56.
57. Glard Y, Launay F, Edgard-Rosa G, Collignon P, Jouve JL, Bollini G. Scoliotic curve patterns in patients with Marfan syndrome. *J Child Orthop*. 2008;2(3):211-216.
58. Qiao J, Xu L, Liu Z, et al. Surgical treatment of scoliosis in Marfan syndrome: outcomes and complications. *Eur Spine J*. 2016;25(10):3288-3293.
59. Sponseller PD, Sethi N, Cameron DE, Pyeritz RE. Infantile scoliosis in Marfan syndrome. *Spine*. 1997;22(5):509-516.
60. Escalada F, Marco E, Duarte E, et al. Growth and curve stabilization in girls with adolescent idiopathic scoliosis. *Spine*. 2005;30(4):411-417.
61. Sponseller PD, Hobbs W, Riley LH 3rd, Pyeritz RE. The thoracolumbar spine in Marfan syndrome. *J Bone Joint Surg Am*. 1995;77(6):867-876.
62. Lipscomb KJ, Clayton-Smith J, Harris R. Evolving phenotype of Marfan's syndrome. *Arch Dis Child*. 1997;76(1):41-46.
63. Scott JC, Morgan TH. The natural history and prognosis of infantile idiopathic scoliosis. *J Bone Joint Surg*. 1955;37-b(3):400-413.
64. Branthwaite MA. Cardiorespiratory consequences of unfused idiopathic scoliosis. *Br J Dis Chest*. 1986;80(4):360-369.
65. Swank SM, Winter RB, Moe JH. Scoliosis and cor pulmonale. *Spine*. 1982;7(4):343-354.
66. Pérez-Machado G, Berenguer-Pascual E, Bovea-Marco M, et al. From genetics to epigenetics to unravel the etiology of adolescent idiopathic scoliosis. *Bone*. 2020;140:115563.
67. Liu J, Zhou Y, Liu S, et al. The coexistence of copy number variations (CNVs) and single nucleotide polymorphisms (SNPs) at a locus can result in distorted calculations of the significance in associating SNPs to disease. *Hum Genet*. 2018;137(6-7):553-567.
68. Kou I, Otomo N, Takeda K, et al. Genome-wide association study identifies 14 previously unreported susceptibility loci for adolescent idiopathic scoliosis in Japanese. *Nat Commun*. 2019;10(1):3685.
69. Qin X, He Z, Yin R, Qiu Y, Zhu Z. Abnormal paravertebral muscles development is associated with abnormal expression of PAX3 in adolescent idiopathic scoliosis. *Eur Spine J*. 2020;29(4):737-743.
70. Zhuang Q, Ye B, Hui S, et al. Long noncoding RNA lncAIS downregulation in mesenchymal stem cells is implicated in the pathogenesis of adolescent idiopathic scoliosis. *Cell Death Differ*. 2019;26(9):1700-1715.
71. Shi B, Mao S, Xu L, et al. Quantitation analysis of PCDH10 methylation in adolescent idiopathic scoliosis using pyrosequencing study. *Spine*. 2020;45(7):E373-E378.
72. Meng Y, Lin T, Liang S, et al. Value of DNA methylation in predicting curve progression in patients with adolescent idiopathic scoliosis. *EBioMedicine*. 2018;36:489-496.
73. Wen J, Liu J, Jiang H, et al. lncRNA expression profiles related to apoptosis and autophagy in peripheral blood mononuclear cells of patients with rheumatoid arthritis. *FEBS Open Bio*. 2020;10(8):1642-1654.
74. Zhou J, Stein P, Leu NA, et al. Accelerated reproductive aging in females lacking a novel centromere protein SYCP2L. *Hum Mol Genet*. 2015;24(22):6505-6514.
75. Yang X, Han H, de Carvalho DD, Lay FD, Jones PA, Liang G. Gene body methylation can alter gene expression and is a therapeutic target in cancer. *Cancer Cell*. 2014;26(4):577-590.
76. Cai T, Hirai H, Zhang G, et al. Deletion of la-2 and/or la-2 β in mice decreases insulin secretion by reducing the number of dense core vesicles. *Diabetologia*. 2011;54(9):2347-2357.
77. Jaiswal RK, Jaiswal N, Bruder SP, Mbalaviele G, Marshak DR, Pittenger MF. Adult human mesenchymal stem cell differentiation to

- the osteogenic or adipogenic lineage is regulated by mitogen-activated protein kinase. *J Biol Chem.* 2000;275(13):9645-9652.
78. Naor Z, Benard O, Seger R. Activation of MAPK cascades by G-protein-coupled receptors: the case of gonadotropin-releasing hormone receptor. *Trends Endocrinol Metab.* 2000;11(3):91-99.
79. Cortizo AM, Lettieri MG, Barrio DA, Mercer N, Etcheverry SB, McCarthy AD. Advanced glycation end-products (AGEs) induce concerted changes in the osteoblastic expression of their receptor RAGE and in the activation of extracellular signal-regulated kinases (ERK). *Mol Cell Biochem.* 2003;250(1-2):1-10.
80. Wang B, Jiang B, Li Y, et al. AKAP2 overexpression modulates growth plate chondrocyte functions through ERK1/2 signaling. *Bone.* 2021; 146:115875.
81. Holm TM, Habashi JP, Doyle JJ, et al. Noncanonical TGF β signaling contributes to aortic aneurysm progression in Marfan syndrome mice. *Science.* 2011;332(6027):358-361.
82. Tashima Y, He H, Cui JZ, et al. Androgens accentuate TGF- β dependent Erk/Smad activation during thoracic aortic aneurysm formation in Marfan syndrome male mice. *J Am Heart Assoc.* 2020;9(20):e015773.
83. Lim WW, Dong J, Ng B, et al. Inhibition of IL11 signaling reduces aortic pathology in murine Marfan syndrome. *Circ Res.* 2022;130(5): 728-740.
84. Li W, Li Y, Zhang L, et al. AKAP2 identified as a novel gene mutated in a Chinese family with adolescent idiopathic scoliosis. *J Med Genet.* 2016;53(7):488-493.
85. Kato N, Loh M, Takeuchi F, et al. Trans-ancestry genome-wide association study identifies 12 genetic loci influencing blood pressure and implicates a role for DNA methylation. *Nat Genet.* 2015;47(11): 1282-1293.

SUPPORTING INFORMATION

Additional supporting information can be found online in the Supporting Information section at the end of this article.

How to cite this article: Zheng, Z., Xu, J., Chen, J., Jiang, B., Ma, H., Li, L., Li, Y., Dai, Y., & Wang, B. (2024). Integrated DNA methylation analysis reveals a potential role for PTPRN2 in Marfan syndrome scoliosis. *JOR Spine*, 7(1), e1304. <https://doi.org/10.1002/jsp2.1304>